The sintering temperature effect on the microstructure and dielectric properties of Bi$_4$Ti$_3$O$_{12}$ doped with neodymium

© *S.V. Zubkov* [1], *I.A. Parinov* [2], *A.V. Nazarenko* [3], *A.V. Pavlenko* [1,3]

[1] Scientific Research Institute of Physics, Southern Federal University,
Rostov-on-Don, Russia
[2] Institute for Mathematics, Mechanics, and Computer Science in the name of I.I. Vorovich,
Southern Federal University,
Rostov-on-Don, Russia,
[3] Federal Research Centre The Southern Scientific Centre of the Russian Academy of Sciences (SSC RAS),
Rostov-on-Don, Russia,

E-mail: svzubkov61@mail.ru

A new set of perovskite-like Bi$_{4-x}$Nd$_x$Ti$_3$O$_{12}$ ($x = 0.1$, 0.3, 0.5, 0.7) oxides were synthesized by the method of high-temperature solid-phase reaction at the temperatures of 1000°C and 1050°C. X-ray diffraction study showed that these compounds are single-phase and have the structure of the Aurivillius phases (AP) family with parameters close to the orthorhombic unit cell corresponding to the space group B2cb (41). The microstructure was studied for all obtained Bi$_{4-x}$Nd$_x$Ti$_3$O$_{12}$ ($x = 0.1$, 0.3, 0.5, 0.7) compositions sintered at temperatures of 1000°C and 1050°C. Its analysis also showed that the crystallites are similar one of AP family and characterized with a lamellar-like shape. The relative permittivity $\varepsilon/\varepsilon_0$ and the dielectric loss tangent tg δ were measured as a function of temperature at frequencies in the range of 100 kHz to 1 MHz.

Keywords: Aurivillius phases, Bi$_{4-x}$Nd$_x$Ti$_3$O$_{12}$, Curie temperature T_C, microstructure, permittivity.

1. Introduction

In 1949, when studying the system Bi$_2$O$_3$– TiO$_2$ V. Aurivillius synthesized oxide Bi$_4$Ti$_3$O$_{12}$ with a perovskite type structure [1,2]. However, at first V. Aurivillius limited himself to studying the structure of the resulting compound. In 1950 Smolensky et al. [3] suggested the occurrence of spontaneous polarization in a perovskite-like layer consisting of octahedra. Only after almost ten years Smolensky et al. [4] discovered ferroelectric properties of Bi$_2$PbNbO$_9$ belonging to this class of compounds. In a few years, several dozen AP were synthesized and almost all of them were ferroelectrics [5,6]. The general formula is A$_{m-1}$Bi$_2$B$_m$O$_{3m+3}$. The crystal structure of AP includes alternating layers [Bi$_2$O$_2$]$^{2+}$ separated by m perovskite-like layers [A$_{m-1}$B$_m$O$_{3m+1}$]$^{2-}$, where A ions have large radii (Bi^{3+} [7], Ca^{2+}, Gd^{3+} [8], Sr^{2+}, Ba^{2+}, Pb^{2+}, Na$^+$, K$^+$, Y^{3+} [9], Ln^{3+}, Nd^{3+} [10], Lu^{3+} [11] (lanthanides)) and demonstrate dodecahedral coordination. Positions B in oxygen octahedra are occupied by highly charged ($\geq 3+$) cations of small radius (Ti^{4+}, V, Nb^{5+}, Ta^{5+} [12], W^{6+} [13], Mo^{6+}, Fe^{3+}, Mn^{4+}, Cr^{3+}, Ga^{3+}, etc.).

The m value is determined by the number of perovskite layers [A$_{m-1}$B$_m$O$_{3m+1}$]$^{2-}$ located between fluorite-like layers [Bi$_2$O$_2$]$^{2+}$ along the pseudotetragonal c-axes [14], and can be an integer or a half-integer in the range $m = 1-5$ (see Fig. 1). Substitutions of atoms in positions A and B significantly affect the electrophysical properties of AP.

In particular, there are large changes in the values of permittivity, electrical conductivity, in addition, the Curie temperature T_C can also vary widely. Thus, the study of cation-substituted AP compounds is of great importance in the development of materials for various technical purposes.

The structure of AP compounds Bi$_2$A$_{m-1}$B$_m$O$_{3m+3}$ above the Curie point T_C is tetragonal and belongs to the space group I4/mmm. The type of space group below the Curie point T_C is determined by the value m. Space group of ferroelectric phase: B2cb or Pca2$_1$ for odd m, A2$_1$am for even m and Cmm2 or I2cm for half-integers m.

Many studies have focused on the use of AP in a non-volatile ferroelectric memory system FeRAM with random access [15] with the potential for wide application in the electronics industry, such as: capacitors and sensors [16]. Bi$_4$Ti$_3$O$_{12}$ (BiT) is one of the most studied compounds of the AP family [17]. Spontaneous polarization Ps of compounds with an even number of layers occurs only along the a-axis. The strong spontaneous polarization of BiT in the ab-plane occurs due to the displacement of Bi atoms in the A-position relative to the octahedron [TiO$_6$] along the a-axis, while non-central displacements Ti in the octahedron for Ps play a minor role, in addition to the large polarization along the a-axis. Recently, bismuth layered structure ferroelectrics (BLSF) have attracted a lot of attention because of their excellent ferroelectric properties and fatigue-free operation. In addition, the

BLSF family is one of the promising lead-free materials from the point of view of their application in functional electronics devices, such as resonators and high-temperature sensors. This is due to the fact that BiT has a high Curie temperature $T_C = 675°C$ and a high residual polarization (P_r) $50\mu C/cm^2$ [18].

However, the main problem in the study of BiT [19–28] was the presence of oxygen vacancies. Oxygen deficiency causes high leakage currents and electrical conductivity values, which can interfere with the polarization process of BiT [29–33] materials. Various synthesis methods were used to improve the properties of BLSF in both thin-film and ceramic forms [34–38]. For thin films, a number of studies have shown that the morphology of grains with a high orientation along the c-axis can be obtained using several processing methods, in particular, by growing grains according to a template, which made it possible to measure the anisotropic properties of these films [39–42]. It is well known in ceramics that both „pure" and doped BLSF have properties that also depend on the orientation of the lamellar grains. For example, the dielectric properties along the directions perpendicular and parallel to the c-axis turned out to be completely different [43]. Therefore, due to the anisotropic behavior of this material, BLSF ceramics were synthesized with grains oriented in a certain direction using various methods, such as grain growth by sample and tape casting [44]. Moreover, using external parameters such as magnetic field or pressure, it was possible to produce ceramics with oriented grains [44]. BiT ceramics with highly oriented grains can be made from pressed plate powders made from salt solutions. However, the resulting ceramics have large pores between well-sintered lamellar colonies of grains. We used a solid-phase reaction pathway for the synthesis of ceramics in this article. In an early study [45], we found that during sintering at different temperatures, significant changes in the crystal structure and the permittivity values occur. The purpose of this work was to study changes in the microstructure and relative permittivity with increasing sintering temperature of $Bi_{4-x}Nd_xTi_3O_{12}$ ($x = 0.1, 0.3, 0.5, 0.7$).

2. Experiment

Polycrystalline AP samples $Bi_{4-x}Nd_xTi_3O_{12}$ ($x = 0.1, 0.3, 0.5, 0.7$) were synthesized by solid-phase reaction of oxides Bi_2O_3, Nd_2O_3, TiO_2. All the initial compounds had the analytically pure qualification. After weighing by stoichiometric composition and grinding of the initial oxides with the addition of ethanol, the pressed samples were calcined at a temperature of $780°C$ for 4 h with intermediate crushing and grinding. The samples were fired in a laboratory muffle furnace in air. Then the samples were crushed, re-crushed and pressed into tablets with a diameter of 10 mm and a thickness of $1.0-1.5$ mm at $1000°C$ (in 2 h) or $1050°C$ (in 2 h). XRD patterns were obtained using a copper X-ray tube. The $CuK\alpha_1, \alpha_2$

radiation was separated from the entire spectrum using a Ni filter. The XRD patterns was measured in the range of angles 2θ from $10°$ to $60°$ with a scanning step of $0.02°$ and a time of intensity (exposure) registration of 12 s per point. The study of the diffractogram profile, determination of the position of the lines, their indexing (hkl) and refinement of the unit cell parameters were carried out using the program PCW2.4 [46]. To measure the dielectric permittivity and electrical conductivity the electrodes were placed on flat surfaces of samples in the form of disks with a diameter of 10 mm and a thickness of about 1.5 mm using Ag paste, which were fired at a temperature of $700°C$ for 30 min. The dependences of the dielectric characteristics on temperature and frequency were determined using an E7-20 immitance meter in the frequency range from 100 kHz to 1 MHz and in the temperature range from room temperature to $900°C$. The samples were polarized in an oil bath at $125°C$ at a voltage of 35 kV/cm for 30 min.

Images of the microstructure of a number of synthesized $Bi_{4-x}Nd_xTi_3O_{12}$ ($x = 0.1, 0.3, 0.5, 0.7$) perovskite-like ceramics obtained using a Carl Zeiss scanning electron microscope EVO 40 (Germany) in the Center for Collective Use of the SSC RAS. The studies were carried out on just made cross-section chips. In the absence of an additional conductive layer, blurring of the grain image and various effects of charge accumulation were observed, especially along the grain boundaries. Therefore, a conductive layer was applied using the SC7620 MiniSputterCoater magnetron sputtering unit to study the chip surface. The samples were not machined before sputtering. The studies were carried out in the mode of high accelerating potential ($EHT = 20$ kV). The probe current $I_{probe} = 20$ pA and the operating distance $WD = 6-8$ mm were used to increase the resolution.

3. Results and their discussion

Powder difractograms of ceramics sintered at $1000°C$ and $1050°C$, in the angle range 2θ $10-60°$, are shown in Fig. 2, 3, respectively. All synthesized solid solutions of $Bi_{4-x}Nd_xTi_3O_{12}$ ($x = 0.1, 0.3, 0.5, 0.7$) correspond to single-phase AP with $m = 3$ and do not contain additional reflexes, which indicates the entry of Nd^{3+} ions into the lattice and the formation of solid solutions.

All studied solid solutions of $Bi_{4-x}Nd_xTi_3O_{12}$ ($x = 0.1, 0.3, 0.5, 0.7$) is isostructural to the well-known perovskite-like $Bi_4Ti_3O_{12}$ compound. The XRD peak (117) on Fig. 1, 2 shows the highest intensity in the plane $(11(2m+1))$. This typical diffraction peak corresponds to a layered BiT structure. It can be seen that the degree of orientation $00l$ of ceramics remains constant and does not depend on the concentration of Nd^{3+}, which is typical when sintering for a short ($t < 25$ h) time. On Fig. 2 it can be seen that the peak (117) shifts towards a larger angle when increasing x from 0.1 to 0.7.
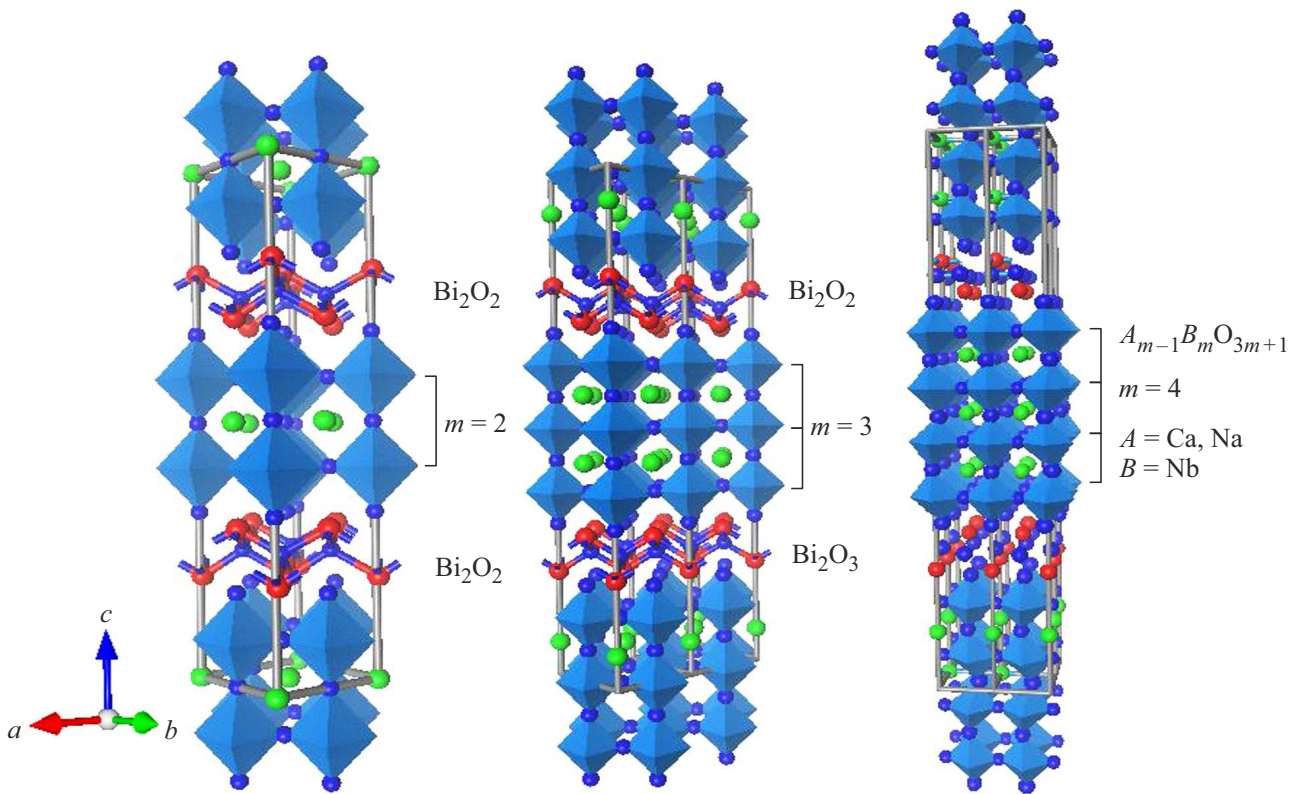
Figure 1. Aurivillius phase structures: $m = 2, 3, 4$.

On the other hand, the orthorhombic BiT structure usually leads to splitting of the peaks $(hkl)/(khl)$ $(h \neq k)$ due to the small difference in the lattice parameters a and b. The diffraction angle of the peak (020) in Fig. 2, b corresponds to the same trend as the peak (117), while the diffraction angle of the peak (200) basically remains unchanged. These two peaks can be associated with the change in the dimensions of the a- and b-axes, respectively. In addition, the distortion of the lattice and the change in the volume of the combined cell may be responsible for the change in the angles of peaks (220) and (115), as shown in Fig. 2, c. The splitting of peak (220) is typical for orthorhombic symmetry [47,48]. However, as in the classical cases for powder samples, the phases are indexed as orthorhombic B2cb when the crystallinity is not high enough and monoclinic distortion is not observed [49].

3.1. Microstructure

The analysis of the images showed that the thermodynamic background of the manufacture of materials strongly influences the morphology of the microstructure. The samples synthesized at a temperature of $1000°C$ are characterized by sufficiently small crystallite sizes (Fig. 4, 5). It can be noted that the bond strength of the grains along the borders is lower than the strength of the grain itself, so the chipping occurred mainly along the borders. The grains acquire a flatter shape with an increase in the amount of neodymium, while being packed into a denser structure. The average crystallite size is about $0.95-1.2\,\mu\text{m}$ at $x = 0.1$ and 0.3, and it equals to about $0.7\,\mu\text{m}$ at $x = 0.5$. The size distribution is lognormal in all cases.

When the sintering temperature increases by only $50°C$ (from $1000°C$ to $1050°C$) the situation is changing significantly (see Fig. 4, 5, b). Firstly, the grains become noticeably larger. At concentrations of $x = 0.1$, 0.3 the growth of the grain sizes was approximately $1.5-2$ times, and at concentrations of $x = 0.5$, 0.7 the growth is more significant — $2.5-3$ times. Secondly, unlike ceramics sintered at $1000°C$, after a temperature of $1050°C$ the chipping occurred mainly along the grains (i. e., the grains themselves were chipped), which indicates an increase in the strength of the intergrain boundaries. This confirms the assumption that the synthesis proceeds with the participation of the liquid phase. Locally it is possible to observe their heterogeneous (layered) structure (Fig. 4, b, d, f arrows). This indicates grain growth along the plane $a-b$ perpendicular to the crystallographic c-axis, which fully corresponds to the structure of the AP type.

Analysis of general statistical data on the crystalliites size range of $\text{Bi}_{3.3}\text{Nd}_{0.7}\text{Ti}_3\text{O}_{12}$ ceramic (see Fig. 5, b) allows to conclude that their distributoin in both cases also obeys the standard logarithmically normal law with an average size of $\sim 1.1\,\mu\text{m}$ (for $T = 1000°C$) and $\sim 2.5\,\mu\text{m}$ ($T = 1050°C$). At the same time, in confirmation of the growth of

the average grain size with an increase in the sintering temperature, it is seen that 93% of the sizes of all grains of ceramics made at $T = 1050°C$ are within $1.5-4\,\mu$m, while for ceramics made at $T = 1000°C$, this range is only $1-2\,\mu$m.
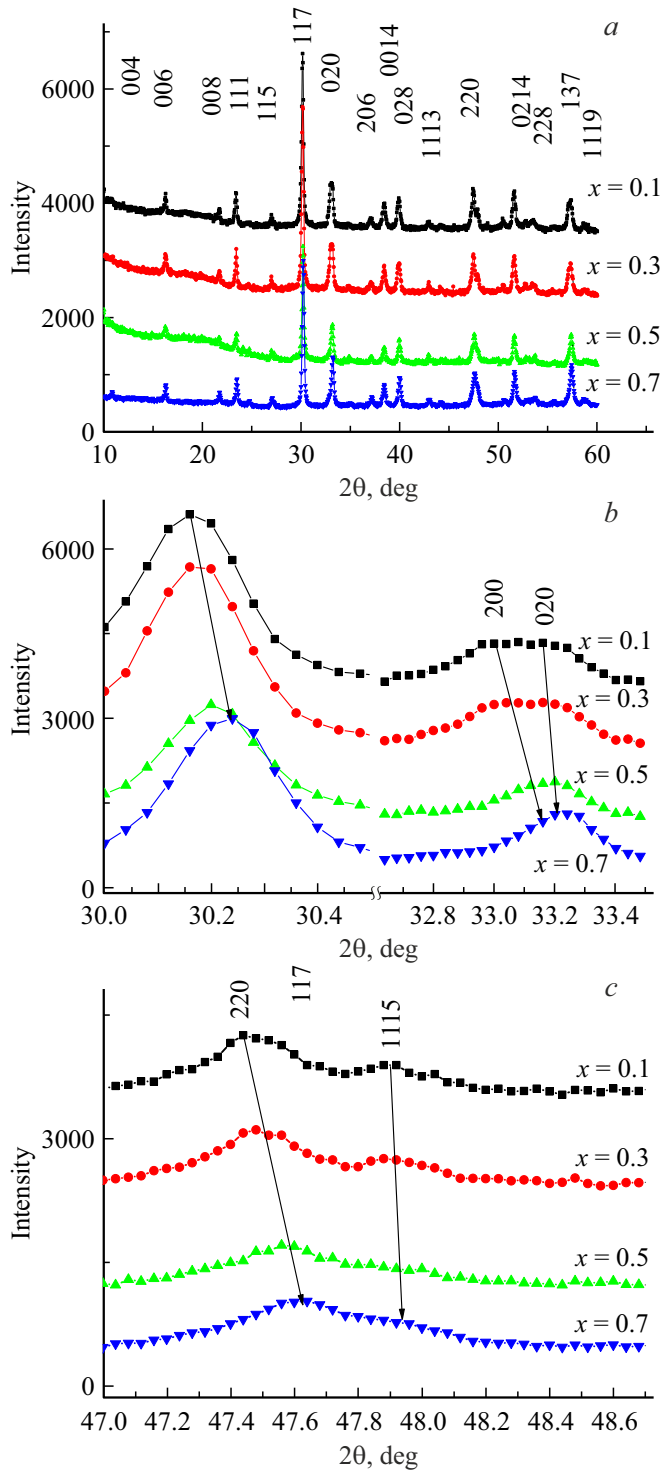

Figure 2. Ceramic diffractograms of Bi$_{4-x}$Nd$_x$Ti$_3$O$_{12}$ ($x = 0.1$, 0.3, 0.5, 0.7), sintered at 1000°C, in the range of angles 2θ of $10°-60°$: *a* — general picture, *b, c* — detailed image of the most characteristic peaks.
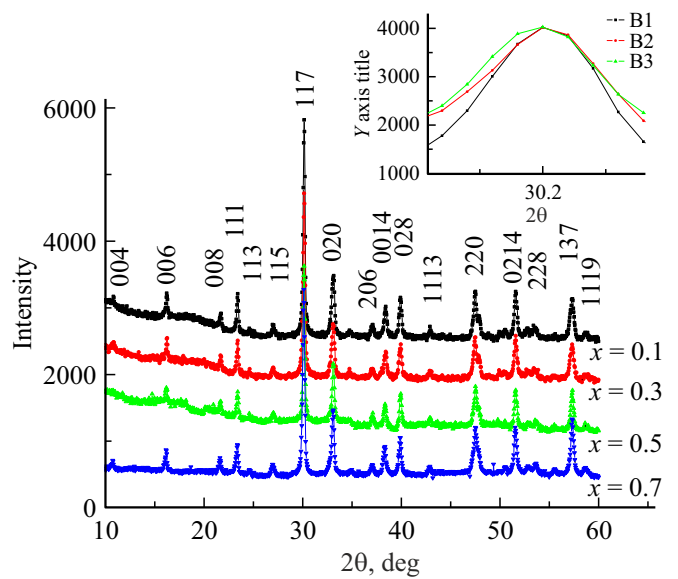
Figure 3. XRD patterns of Bi$_{4-x}$Nd$_x$Ti$_3$O$_{12}$ ($x = 0.1$, 0.3, 0.5, 0.7) ceramics, sintered at 1050°C, in the angle range 2θ $10°-60°$.

3.2. Dielectric properties

Figure 6 shows the dependences of the relative permittivity $\varepsilon/\varepsilon_0$ and the tangent of the dielectric loss angle $\mathrm{tg}\,\delta$ on the temperature for Bi$_{4-x}$Nd$_x$Ti$_3$O$_{12}$ ($x = 0.1$, 0.3, 0.5, 0.7) AP at frequency values from 100 kHz to 1 MHz for ceramics sintered at temperatures of 1000°C and 1050°C. As can be seen from Fig. 6, a significant decrease in the Curie temperature T_C (from 695°C to 580°C) is associated with the doping of Nd^{3+}.

Fig. 6 shows that the tangent of the dielectric loss angle for the Bi$_{4-x}$Nd$_x$Ti$_3$O$_{12}$ ($x = 0.1$) composition increases by 1.5 times with an increase in the heating of samples from 1000°C to 1050°C. As is known, Bi^{3+} „escapes" at a temperature of $T > 1000°C$ and oxygen vacancies are formed. Bi^{3+} vacancies are formed mainly in the A-positions of the perovskite-like layer, and not in the layers Bi$_2$O$_2^{2+}$, which leads to the formation of oxygen vacancies in the perovskite-like layer.

The increase in the value of the tangent of the dielectric loss angle $\mathrm{tg}\,\delta$ is explained by the fact that the electrical conductivity along the *a*-axis is several orders of magnitude greater than along the *c*-axis. Oxide-ion conductivity is attributable to a large number of oxygen vacancies in perovskite-like layers, which leads to a large conductivity along the *a*-axis at 700°C, in case of measurement of the relative permittivity $\varepsilon/\varepsilon_0(T)$ with a temperature change. As shown in Fig. 4, *a, b*, the grain sizes in the *ab*-plane increase with an increase of the sintering temperature, which leads to an increase of conductivity and an increase of the tangent of the dielectric loss angle for Bi$_{4-x}$Nd$_x$Ti$_3$O$_{12}$ ($x = 0.1$) (Fig. 6, *a, b*).

Further doping of the Bi$_{4-x}$Nd$_x$Ti$_3$O$_{12}$ composition with Nd^{3+} ions leads to a decrease in the tangent of the

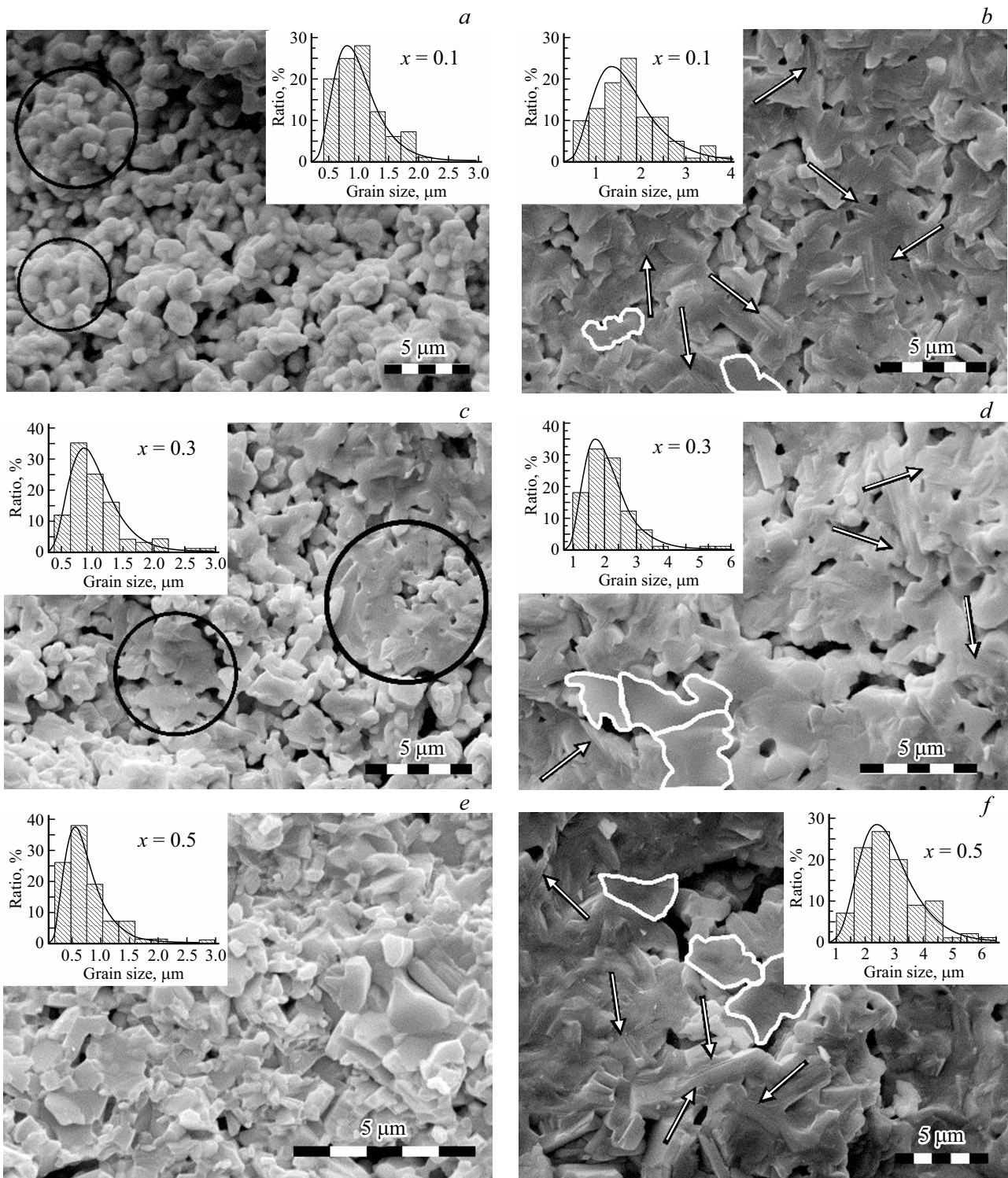**Figure 4.** Microstructure of $Bi_{4-x}Nd_xTi_3O_{12}$ ceramic cross-section after synthesis at $1000°C$ (a, c, e) and at $1050°C$ (b, d, f). The following inserts show histograms of the corresponding grain size distributions.

dielectric loss angle by 2 times, which indicates a decrease in concentrations of oxygen vacancies. High temperature anomaly of relative permittivity $\varepsilon/\varepsilon_0$ is clearly observed over the entire series of $Bi_{4-x}Nd_xTi_3O_{12}$ ($x = 0.1, 0.3, 0.5, 0.7$) synthesized compounds which corresponds to the transition

from tetragonal to orthorhombic state. A low-temperature anomaly of the relative permittivity $\varepsilon/\varepsilon_0$ measured in the temperature range of $200-600°C$ is also observed. Low-temperature dielectric anomaly for $Bi_{4-x}Nd_xTi_3O_{12}$ ($x = 0.1, 0.3, 0.5, 0.7$) is a combination of relaxation peaks
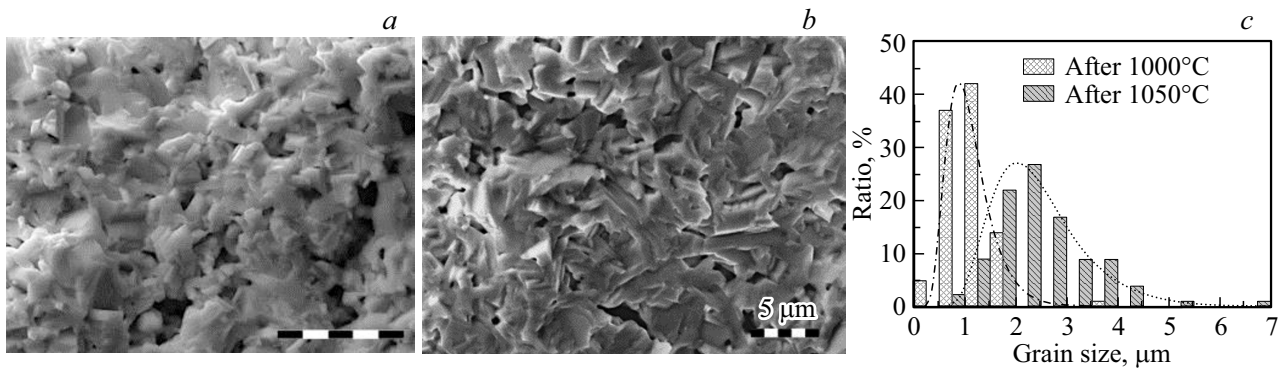
Figure 5. Microstructure of $Bi_{3.3}Nd_{0.7}Ti_3O_{12}$ ceramic cross-section after synthesis at $1000°C$ (*a*) and $1050°C$ (*b*) and a comparative histogram of the temperature evolution of their grain size distributions (*c*).
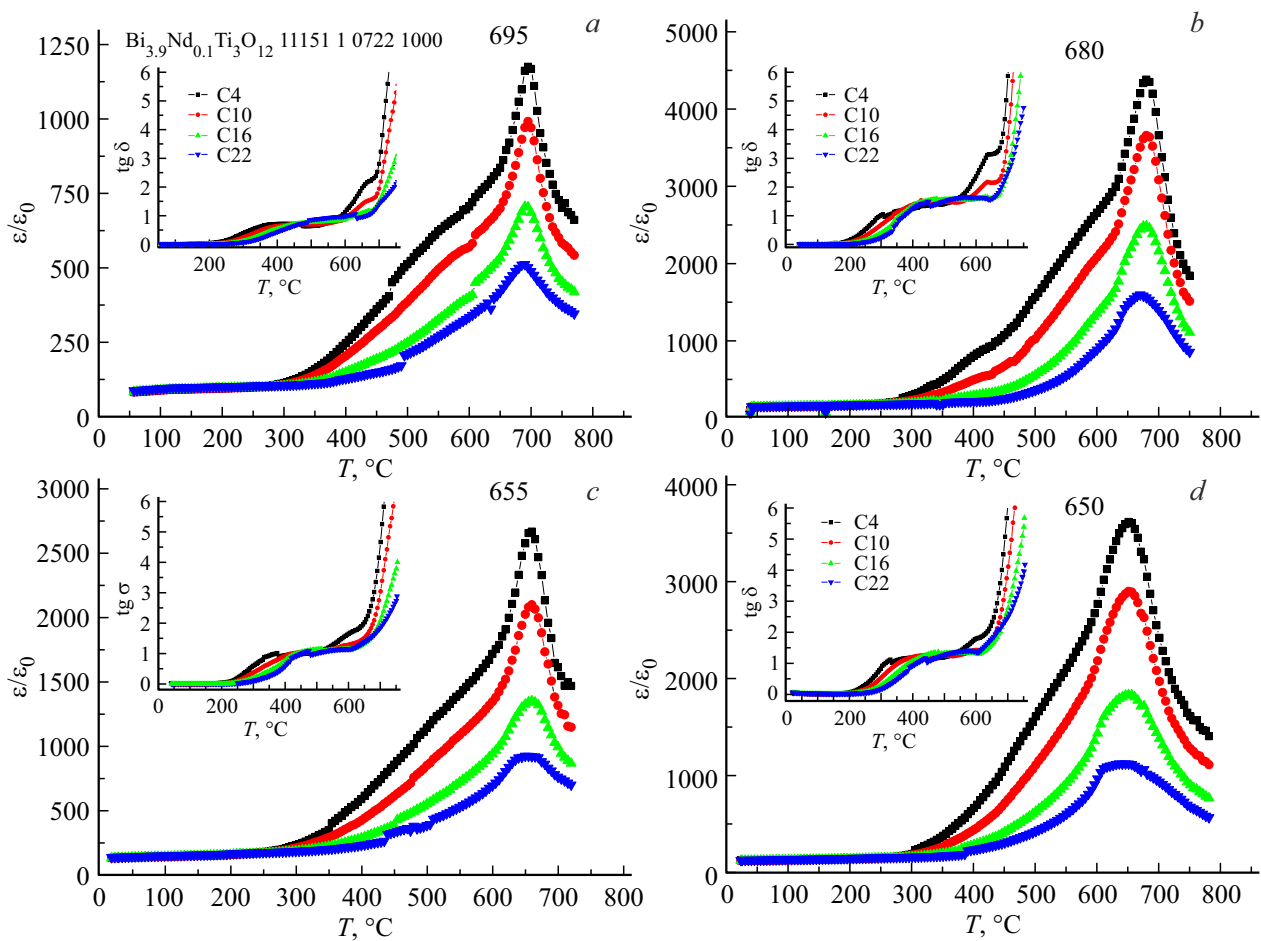

Figure 6. Temperature-frequency dependences of the relative permittivity $\varepsilon/\varepsilon_0$ and the tangent of the dielectric loss angle $\operatorname{tg}\delta$ (inserts) for AP of $Bi_{4-x}Nd_xTi_3O_{12}$ ($x = 0.1$ (*a, b*), 0.3 (*c, d*), 0.5 (*e, f*), 0.7 (*g, h*)) after synthesis at $1000°C$ (*a, c, e, g*) and $1050°C$ (*b, d, f, h*) in the frequency range from $100\,\mathrm{kHz}$ to $1\,\mathrm{MHz}$ and temperatures $25-750°C$.

that depend on the frequency, which is consistent with the results of H.S. Shulman et al. [22].

As can be seen from Fig. 6, *c, d* a frequency shift of the maxima relative permittivity is observed with increasing concentration of Nd^{3+} ions more then $x = 0.3$, which corresponds to the appearance of relaxor states. The maxima of the relative permittivity are diffused over the temperature. Relaxation in the temperature range from $200°C$ to $500°C$ is probably associated with the displacement of oxygen anions over short distances in the crystal or with the formation of Schottky barriers between „ceramic" and metal electrodes due to the difference in Fermi levels between them [50].
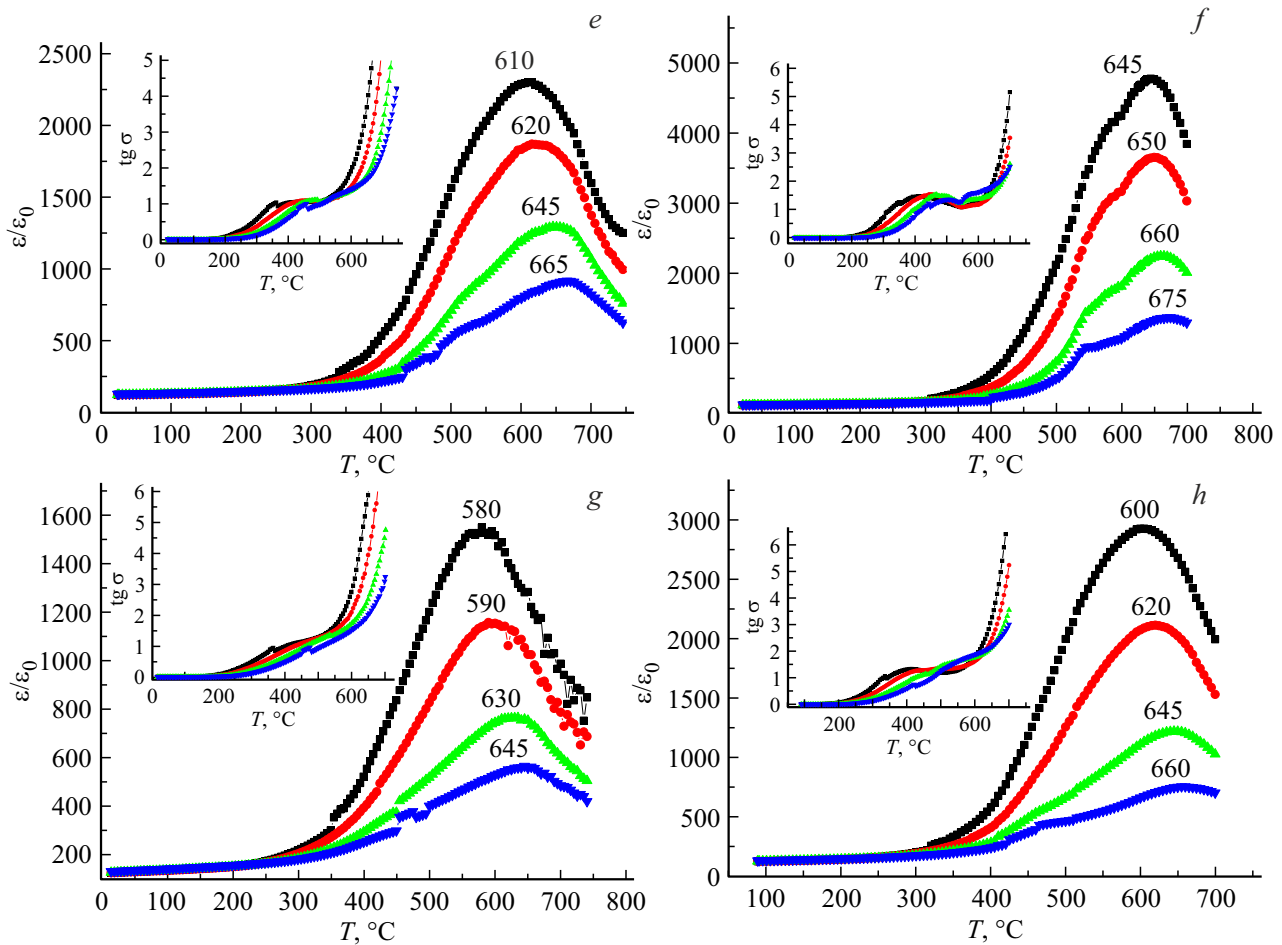
Fig. 6 (*continued*).

Table 1. Lattice cell parameters a_0, b_0, c_0, V; a_t — average tetragonal period, c' — height of the octahedron along the c-axis, $\delta c'$ — deviation from the cubic shape, δb_0 — rhombic distortion for ceramics sintered at a temperature of $1000°C$

Compound	a_0, Å	b_0, Å	c_0, Å	V_{1000}, Å^3	δb_0	c'	a_t	$\Delta c'$
$Bi_{3.9}Nd_{0.1}Ti_3O_{12}$	5.405	5.436	32.824	964.242	0.061	4.103	3.830	0.070
$Bi_{3.7}Nd_{0.3}Ti_3O_{12}$	5.403	5.439	32.805	963.246	0.066	4.100	3.830	0.070
$Bi_{3.5}Nd_{0.5}Ti_3O_{12}$	5.405	5.419	32.815	961.141	0.026	4.101	3.826	0.070
$Bi_{3.3}Nd_{0.7}Ti_3O_{12}$	5.399	5.419	32.817	960.133	0.037	4.102	3.826	0.070

Table 2. Lattice cell parameters a_0, b_0, c_0, V; a_t — average tetragonal period, c' — height of the octahedron along the c-axis, $\delta c'$ — deviation from the cubic shape, δb_0 — orthorhombic distortion for ceramics sintered at a temperature of $1050°C$

Compound	a_0, Å	b_0, Å	c_0, Å	V_{1050}, Å^3	t	δb_0	c'	a_t	$\Delta c'$
$Bi_{3.9}Nd_{0.1}Ti_3O_{12}$	5.409	5.430	32.821	963.746	0.979	0.388	4.103	3.830	0.070
$Bi_{3.7}Nd_{0.3}Ti_3O_{12}$	5.405	5.430	32.813	963.033	0.976	0.462	4.101	3.830	0.070
$Bi_{3.5}Nd_{0.5}Ti_3O_{12}$	5.404	5.410	32.798	958.160	0.974	0.110	4.099	3.823	0.070
$Bi_{3.3}Nd_{0.7}Ti_3O_{12}$	5.400	5.412	32.790	958.120	0.971	0.220	4.098	3.822	0.070

Table 3. Values of tolerance factor t, Curie temperature T_C, relative permittivity and activation energy $E_{1,2}$ for Bi$_{4-x}$Nd$_x$Ti$_3$O$_{12}$ ($x = 0.1$, 0.3, 0.5, 0.7) ceramics, sintered at $1000°$C and $1050°$C

	Compound	t-factor	T_{C1000}/T_{C1050}	$\varepsilon'_{1000}/\varepsilon'_{1050}$	E_1/E_2, eV at $1000°$C	E_1/E_2, eV at $1050°$C
1	Bi$_{3.9}$Nd$_{0.1}$Ti$_3$O$_{12}$	0.978	695/680	1250/5000	0.56/0.04	0.50/0.03
2	Bi$_{3.7}$Nd$_{0.3}$Ti$_3$O$_{12}$	0.976	655/650	2805/3619	0.55/0.05	0.56/0.02
3	Bi$_{3.5}$Nd$_{0.5}$Ti$_3$O$_{12}$	0.974	610/645	2300/4800	0.54/0.03	0.59/0.05
4	Bi$_{3.3}$Nd$_{0.7}$Ti$_3$O$_{12}$	0.971	580/600	1600/3000	0.56/0.02	0.58/0.06

BiT ceramics had low piezoactivity ($d_{33} \leq 8$ pC/N), doping of Nd^{3+} did not cause any change it. The temperature dependence of dielectric permittivity of Bi$_{4-x}$Nd$_x$Ti$_3$O$_{12}$ ($x = 0.1$, 0.3, 0.5, 0.7) samples was measured again after polarization. It was found that the Curie temperature T_C decreased by $10°$C.

The parameters and volume of the unit cell were determined on the basis of X-ray diffraction analysis data; they are given in Table 1 (for temperature $1000°$C) and Table 2 (for temperature $1050°$C).

Obtained unit cell parameters for samples Bi$_{4-x}$Nd$_x$Ti$_3$O$_{12}$ ($x = 0.1$, 0.3, 0.5, 0.7) are close to those previously defined for the Bi$_4$Ti$_3$O$_{12}$ AP [38]: $a = 5.411$ Å, $b = 5.448$ Å, $c = 32.81$ Å. We determined the tolerance factor t, presented in Table 3 to obtain the degree of distortion of the ideal perovskite structure. The tolerance factor t was introduced by V.M. Goldschmidt [51], as a geometric criterion determining the degree of stability and distortion of the crystal structure

$$t = (R_A + R_O)/\left[\sqrt{2}(R_B + R_O)\right], \qquad (1)$$

where R_A and R_B — radii of cations in A- and B-positions, respectively; R_O — ionic radius of oxygen. Here we calculated the tolerance coefficient using the Shannon ionic radii [52], for the corresponding coordination numbers (CN) (CN $= 6$ for O$_2$, $R_O = 1.40$ Å; CN $= 12$ for Nd^{3+}, $R_{Nd}^{3+} = 1.27$ Å; CN $= 6$ for Ti^{4+}, $R_{Ti}^{4+} = 0.605$ Å).

R.D. Shannon did not provide the ionic radius Bi^{3+} for coordination with CN $= 12$. Therefore, its value was determined from the ionic radius with CN $= 8$ ($R_{Bi3+} = 1.17$ Å) multiplied by the approximation coefficient 1.179; then for Bi^{3+} (CN $= 12$) we got $R_{Bi3+} = 1.3$ Å. Tables 1, 2 show the parameters of rhombic δb_0 and tetragonal $\delta c'$ deformation; the average tetragonal period at the average power of one perovskite layer c'; $c' = 3c/(8 + 6m)$ — height of a single perovskite-like layer, $a_t = (a_0 + b_0)/2$ — average value of the tetragonal period; a_0, b_0, c_0 — lattice parameters; $\delta c' = (c' - a_t)/a_t$ — deviation of the shape of an elementary cell from a cubic one, that is, elongation or compression; $\delta b_0 = (b_0 - a_0)/a_0$ — orthorhombic deformation, $c_0 = c/(2 + 1.5m)$ — thickness of the bismuth oxygen layer [53]. The activation energy of E_a of the

conductivity was determined from the Arrhenius equation

$$\sigma = (A/T) \exp\left[-E_a/(kT)\right], \qquad (2)$$

where σ — electrical conductivity, k — Boltzmann constant, A — constant, E_a — activation energy. The dependence of $\ln \sigma$ (σ-conductivity) on $1/T$ (at a frequency of 100 kHz), used to determine the activation energy of E_a, is shown in Fig. 7 for Bi$_{4-x}$Nd$_x$Ti$_3$O$_{12}$ ($x = 0.1$, 0.3, 0.5, 0.7) AP. Compounds of Bi$_{4-x}$Nd$_x$Ti$_3$O$_{12}$ ($x = 0.1$, 0.3, 0.5, 0.7) demonstrate two temperature ranges where the activation energy of the conductivity E_a differs significantly in magnitude. The electrical conductivity in the low temperature range is determined mainly by impurity defects with very low activation energies of conductivity-on the order of hundredths of an electronvolt. For Bi$_{4-x}$Nd$_x$Ti$_3$O$_{12}$ ($x = 0.1$, 0.3, 0.5, 0.7) compounds an area with pronounced impurity conductivity is observed in the temperature range from $20°$C to $200°$C.

When Bi$_4$Ti$_3$O$_{12}$ is doped with neodymium, the activation energy of conductivity practically does not change in the low-temperature and high-temperature regions (see Table 3). The invariance of the activation energy of conductivity indicates the constancy of the nature of conductivity
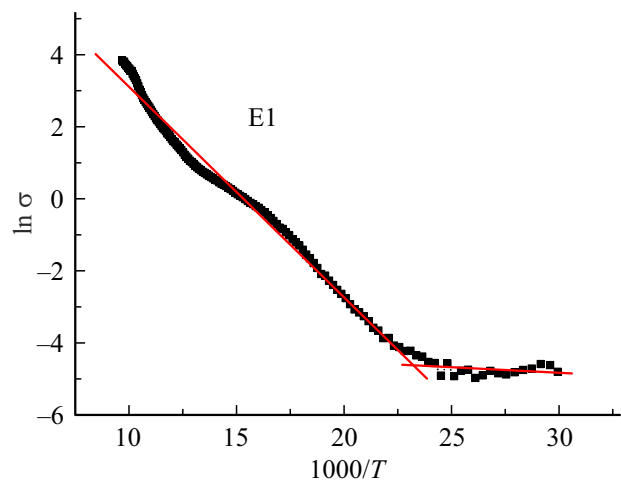
Figure 7. Dependence $\ln \sigma$ on $10000/T$ for Bi$_{4-x}$NdxTi$_3$O$_{12}$ ($x = 0.1$, 0.3, 0.5, 0.7) sample with $x = 0.1$ at 100 kHz.

in a number of $Bi_{4-x}Nd_xTi_3O_{12}$ ($x = 0.1$, 0.3, 0.5, 0.7) synthesized compounds.

4. Conclusion

Tested on a close to Aurivillius phases [38,47–50] studies of the electrophysical properties of $Bi_{4-x}Nd_xTi_3O_{12}$ ($x = 0.1$, 0.3, 0.5, 0.7) perovskite-like oxides are developed in this work. Thus, the ceramics were made using the traditional method of solid-phase reaction. The radiographs were indexed as orthorhombic B2cb for all AP's. As expected, Nd^{3+} doping reduced the tangent of the dielectric loss angle by two times compared to the unalloyed $Bi_4Ti_3O_{12}$. Minimum Curie temperature $T_C = 580°C$ for the synthesized series of $Bi_{4-x}Nd_xTi_3O_{12}$ ($x = 0.1$, 0.3, 0.5, 0.7) compounds was achieved for $Bi_{4-x}Nd_xTi_3O_{12}$ at $x = 0.1$.

Nd^{3+} doping reduces the Curie temperature with an increase of x. The values of the relative permittivity $\varepsilon/\varepsilon_0$ for all samples sintered at $1050°C$ were $1.5-2$ times greater than for samples sintered at $1000°C$. All samples were characterized by an increase in grain size with an increase in sintering temperature. The activation energy of conductivity in the low-temperature and high-temperature regions practically did not change when $Bi_4Ti_3O_{12}$ was doped with Nd^{3+} as follows from Table 3.

Conflict of interest

The authors declare that they have no conflict of interest.

References

[1] B. Aurivillius. Arkiv. Kemi **1**, 499 (1949).

[2] B. Aurivillius. Arkiv. Kemi **37**, 512 (1950).

[3] G.A. Smolensky, R.V. Kozhevnikova. DAN SSSR **76**, 4, 519 (1951). (in Russian).

[4] G.A. Smolensky, V.A. Isupov, A.I. Agranovskaya, S.N. Popov. Sov. fizika tverdogo tela **1**, 169 (1959). (in Russian).

[5] E.C. Subbarao. Phys. Rev. **122**, 3, 804 (1961).

[6] E.C. Subbarao. J. Am. Ceram. Soc. **45**, 166 (1962).

[7] S.V. Zubkov. J. Adv. Dielectrics, **11**, 2160018 (2021), DOI:10.1142/S2010135X21600183

[8] S.V. Zubkov. J. Adv. Dielectrics **10**, *1−2*, 2060002 (2020). DOI:10.1142/S2010135X20600024.

[9] S.V. Zubkov, V.G. Vlasenko. FTT **59**, 12 (2017). (in Russian). DOI: 10.21883/FTT.2017.12.45224.133.

[10] S.V. Zubkov, I.A. Parinov, A.V. Nazarenko, Yu.A. Kuprina. Phys. Solid State **64**, 10 (2022).

[11] S.V. Zubkov, S.I. Shevtsova. Part of the Springer Proc. Materials book series **6**, 173−182 (2020).

[12] S.V. Zubkov. DOI:10.1142/S2010135X20600085

[13] S.V. Zubkov, V.G. Vlasenko, V.A. Shuvaeva, S.I. Shevtsova. FTT **58**, 1 (2016). (in Russian).

[14] C. A.-Pazde Araujo, J.D. Cuchiaro, L.D. McMillan, M.C. Scott, J.F. Scott. Nature London **374**, 627 (1995).

[15] B.H. Park, B.S. Kang, S.D. Bu, T.W. Noh, J. Lee, W. Jo. Nature London **401**, 682 (1999).

[16] L. Pardo, A. Castro, P. Millan, C. Alemany, R. Jimenez, B. Jimenez. Acta Mater. **48**, 2421 (2000).

[17] R.L. Withers, J.G. Thompson, A.D. Rae. J. Solid State Chem. **94**, 404 (1991).

[18] S.E. Cummins, L.E. Cross. J. Appl. Phys. **39**, 2268 (1968).

[19] R. Takahashi, Y. Yonezawa, M. Ohtani, M. Kawasaki, K. Nakajima, T. Chikyow, H. Koinuma, Y. Matsumoto. Adv. Fun. Mater. **16**, 485 (2006).

[20] U. Chon, H.M. Jang, M.G. Kim, C.H. Chang. Phys. Rev. Lett. **89**, 87601 (2002).

[21] J.Y. Choi, C.H. Choi, K.-H. Cho, T.G. Seong, S. Nahm, C.Y. Kang, S.J. Yoon, J.-H. Kim. Acta Mater. **57**, 2454 (2009).

[22] H.N. Lee, D. Hesse, N. Zakharov, U. Gosele. Science **296**, 2006 (2002).

[23] H. Irie, H. Saito, S. Ohkoshi, K. Hashimoto. Adv. Mater. **17**, 491 (2005).

[24] K. Yamamoto, Y. Kitanaka, M. Suzuki, M. Miyayama, Y. Noguchi, C. Moriyoshi, Y. Kuroiwa. Appl. Phys. Lett. **91**, 162909 (2007).

[25] C.B. Long, Q. Chang, H.Q. Fan. Sci. Rep. **7**, 4193 (2017).

[26] H. Watanabe, T. Kimura, T. Yamaguchi. Am. Ceram. Soc. Bull. **74**, 139 (1991).

[27] J. Liu, Z. Shen, M. Nygren, Y. Kan, P. Wang. J. Eur. Ceram. Soc. **23**, 3233 (2006).

[28] M. Takahash, Y. Noguchi, M. Miyayam. Jpn. J. Appl. Phys. **42**, 6222 (2003).

[29] H.S. Shulman, D. Damjanovic, N. Setter. J. Am. Ceram. Soc. **83**, 528 (2000).

[30] M. Takahashia, Y. Noguchi, M. Miyayam. Solid State Ion. **172**, 325 (2004).

[31] H.S. Shulman, M. Testorf, D. Damjanovic, N. Setter. J. Am. Ceram. Soc. **79**, 3124 (1996).

[32] C.B. Long, H.Q. Fan, M.M. Li, G.Z. Dong, Q. Li. Scr. Mater. **75**, 70 (2014).

[33] C. Long, B. Wang, W. Ren, K. Zheng, H. Fan, D. Wang, L. Liu. Appl. Phys. Lett. **117**, 032902 (2020).

[34] L. Shen, D. Xiao, J. Zhu, P. Yu, J. Zhu, D. Gao. J. Mater. Syn. Proc. **9**, 369 (2001).

[35] A.Z. ??, C. Quinelato, A. Ries, B.D. Stojanovic, E. Longo, J.A. Varela. Mater. Chem. Phys. **98**, 481 (2006).

[36] S.W. Kang, M.K. Song, S.W. Rhee, J.H. Suh, C.G. Park. Integr. Ferroelectrics **72**, 61 (2005).

[37] B.D. Stojanovic, A.Z. Simões, C.O. Paiva-Santos, C. Quinelato, E. Longo, J.A. Varela. Ceram. Int. **32**, 707 (2006).

[38] Y. Kan, X. Jin, G. Zhang, P. Wang, Y.B. Cheng, D. Yan. J. Mater. Chem. **14**, 3566 (2004).

[39] P.-H. Xiang, Y. Kinemuchi, K. Watari. J. Eur. Ceram. Soc. **27**, 663 (2007).

[40] U. Chon, H.M. Jang, I.W. Park, Solid State Commun. **127**, 469 (2003).

[41] J.C. Bae, S.S. Kim, E.K. Choi, T.K. Song, W.J. Kim, Y.I. Leed, Thin Solid Films. **472**, 90 (2005).

[42] Y. Kan, P. Wang, Y. Li, Y.-B. Cheng, D. Yan. J. Eur. Ceram. Soc. **23**, 2163(2003).

[43] W. Chen, Y. Kinemuchi, T. Tamura, K. Miwa, K. Watari. Mater. Res. Bull. **41**, 2094 (2006).

[44] W. Chen, Y. Hotta, T. Tamura, K. Miwa, K. Watari. Scripta Mater. **54**, 2063 (2006).

[45] SV. Zubkov, I.A. Parinov, A.V. Nazarenko, Y.A. Kuprina. Physics and Mechanics of New Materials and Their Applications–Proceedings of the International Conference PHENMA 2021-2022, Springer Proceedings in Materials / Eds I.A. Parinov, S.-H. Chang, A.N. Soloviev. Springer Nature, Switzerland **20**, 163 (2023).

[46] W. Kraus, G. Nolze. Powder Cell for Windows 2.39, Federal Institute for Materials Research and Testing, Berlin (1999).

[47] H.L. Du, W.C. Zhou, F. Luo, D.M. Zhu. Appl. Phys. Lett. **91**, 202907 (2007).

[48] Z.P. Yang, Y.F. Chang, B. Liu, L.L. Wei, Mater. Sci. Eng. A **432**, 292 (2006).

[49] R.E. Newnham, R.W. Wolf, J.F. Dorrian, Mat. Res. Bull. **6**, 1029 (1971).

[50] M. Li, Z. Shen, M. Nygren, A. Feteira, D.C. Sinclair, A.R. West. J. Appl. Phys. **106**, 04106 (2009).

[51] V.M. Goldschmidt. Geochemische Verteilungsgesetze der Elemente, J. Dybwad, Oslo, 1923 (1927).

[52] R.D. Shannon, Acta Crystallogr. A **32**, 751 (1976).

[53] V.A. Isupov. Ferroelectrics **189**, 211 (1996).

Translated by A.Akhtyamov